Computation of Hysteresis Torque and Losses in a Bearingless Synchronous Reluctance Machine

Anouar Belahcen[1,2], *Senior Member, IEEE*, Victor Mukhrejee[1], Floran Martin[1], and Paavo Rasilo[1,3]

[1]Aalto University, Dept. of Electrical Engineering and Automation, POBox 15500, Aalto-00076
[2]Tallinn University of Technology, Dept. of Electrical Engineering, Tallinn, Estonia
[3]Tampere University of Technology, Laboratory of Electrical Energy Engineering, Tampere, Finland

This paper presents the methodology and computation results for the torque and iron losses in a bearingless synchronous reluctance machine. The aim is to compute the hysteresis torque related to the asynchronous operation of the machine under the effect of the levitation field rotating at twice the synchronous speed. For this purpose, and because it is impossible to compute the hysteresis torque with a single-valued BH-characteristic, a magneto-dynamic vector hysteresis model is used. The computations show that the hysteresis -related shaft power is considerable under no-load operation of the machine. It is also shown that the asynchronous torque can be approximated by the classical equivalent circuit of an induction machine.

***Index Terms*— Electrical machine, finite element analysis, magnetic hysteresis, magnetic levitation, magnetic losses.**

I. Introduction

Synchronous reluctance machines are nowadays commercialized owing to their robust construction, efficient operation, and inexpensive materials used for their manufacturing. They are intended to achieve the IE4 efficiency class [1]. The design methodology of such machines is also well-established [2]. A novel use of these machines has been expanding lately; it consists of making them bearingless. Bearingless machines integrate the torque production and the magnetic levitation in the core of the machine and remove the need for additional mechanical or magnetic bearings [3]. The operation of a bearingless machine is based on the use of a p-pole-pair rotating field for the torque production and a $p\pm1$-pole-pair for the levitation of the rotor of the machine [3]. The levitation is enabled by the unbalanced magnetic pull created by the additional winding. Bearingless machines can be of different types, but in this paper, we focus on the synchronous reluctance machine (SynRM) where the torque is produced by a 4-pole winding and the levitation force is produced by an additional 2-pole winding, both supplied at 50 Hz.

The primary focus of the research on bearingless machines has been centered on the topology and the control of the machines [3]-[6]. The main assumption for the additional winding is that it does not have any influence on the torque production, as for a synchronous machine to produce a torque, the flux needs to rotate at the same speed as the rotor. However, since the flux of the levitation winding produces eddy currents and hysteresis in the rotor, it has to produce also an asynchronous torque as in the case of an induction or hysteresis machine. As per the best knowledge of the authors, there have been no studies on the effect of the levitation flux on the torque production for synchronous bearingless machines. The aim of this paper is to investigate the effect of the levitation field on the torque production of a synchronous reluctance machine with a 4-pole main winding and a 2-pole levitation winding.

Indeed, a bearingless machine can be illustrated as shown in Fig. 1, where it is divided into a fundamental synchronous machine with respect to the torque-producing field and an asynchronous hysteresis machine with respect to the levitation field. Furthermore, both field harmonics can produce synchronous or asynchronous torque components, either positive or negative. Since the levitation field is rotating at twice the rotor speed (in this particular case), the slip related to this field is very high and equal to 50%. Together with the hysteretic behavior of the rotor material and the eddy currents in the iron sheets, such a field causes the machine to operate as an asynchronous hysteresis machine. The computation of the torque and power related to this operation mode requires special attention.

The conductivity of the rotor materials of a SynRM is usually assumed to be zero in the field equations. Moreover, the hysteresis effects are neglected [7]. Such a modelling methodology cannot catch the effect of the additional winding on the production of asynchronous torque. Therefore, hysteresis and eddy-current models are required in the field equations. Several hysteresis models have been proposed in [8]-[12], but some of them are only scalar, while others do not account for the dynamic effects such as eddy currents, or are very complex to be identified. In this paper, we propose to use a previously developed and validated magneto-dynamic vector hysteresis (MDVH) model [10] to estimate the hysteresis torque and the power transferred from the asynchronous field to the rotor when it is under self-levitation mode. The model accounts for the static hysteresis and eddy currents under both alternating and rotating fields. Besides the torque and power, the model is also used to determine the different components of iron losses in both the stator and the rotor of the machine.

Manuscript received April 1, 2015; revised May 15, 2015 and June 1, 2015; accepted July 1, 2015. Date of publication July 10, 2015; date of current version July 31, 2015. (Dates will be inserted by IEEE; "published" is the date the accepted preprint is posted on IEEE Xplore®; "current version" is the date the typeset version is posted on Xplore®). Corresponding author: A. Belahcen (e-mail: anouar.belahcen@aalto.fi).

Color versions of one or more of the figures in this paper are available online at http://ieeexplore.ieee.org.

Digital Object Identifier (inserted by IEEE).

Finally, the asynchronous shaft power is compared with the one calculated from a classical equivalent circuit approximation for asynchronous machines. A simple experimental proof of concept is also presented. It consists of operating the machine in asynchronous mode with a low voltage supply.

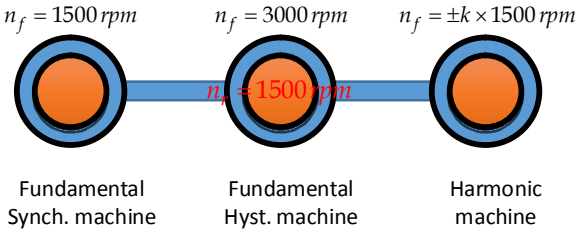

Fig. 1. Illustration of the operation of the bearingless synchronous machine from the point of view of the rotating fields. The rotor speed of the 3 virtual machines is the same. The power produced by the middle part is in the focus of this paper.

II. Hysteresis Model

The MDVH model used in this work consists of a history dependent hysteresis model [11], [12] augmented with the classical eddy current contribution [8], [12]. The whole model is vectorized in sixteen directions according to the Mayergoyz methodology [13], which makes it possible to account for rotational hysteresis. The model is further incorporated into an in-house 2D time stepping finite element software for the simulation of rotating electrical machines. In previous works [10], we validated the Preisach model for the scalar part and a polynomial power function for the eddy current part, but the parameters of these models turned out to be very sensitive to the material used and the model is time consuming. The use of the classical eddy current formulation is justified by the low frequency and the absence of high harmonics. The same methodology is applied in this paper. The excess contribution is omitted from the present model. This is justified by the large airgap in the machines under investigation and the measurements from [14]. Furthermore, the concept of excess losses is clear in the case of alternating field but is still not well understood for the case of rotating fields. The scalar hysteresis model has been identified from measurements with a single sheet tester. The measurement results and the setup are described in [14]. A full description of the scalar model is given in [11], [12] and the description of the vectorization procedure is given in [10].

III. Simulation Model

The machine under investigation is a prototyped bearingless synchronous reluctance motor with a 4-pole main winding and a 2-pole levitation winding. The geometry of the machine with the respective mesh is shown in Fig. 3. The time stepping simulation is carried out while accounting for voltage supply by coupling the field and circuit equations [7].

The computations have been carried out by modeling the magnetic material with a single value (SV) BH-curve and with the above-described MDVH model so that the differences can be identified in the torque production. Contrary to the current supply methodology, the voltage supply ensures that the flux density in the machine airgap is almost the same for both models, provided the same voltage and load angle are used in the simulations. The difference between the simulation results is then seen in the computed input power and power factor. The parameters for the machine are given in Table I.

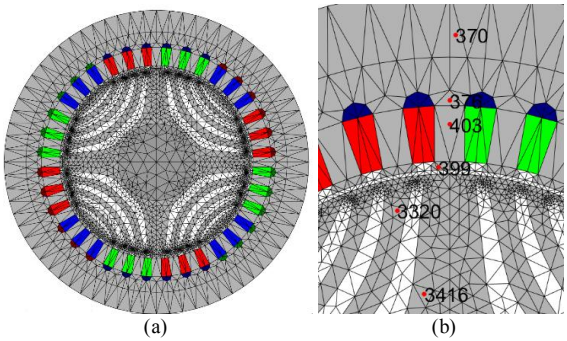

Fig. 2 a) The geometry and the mesh of the bearingless SynRM. The additional winding can be seen at the bottom of the slots. b) The elements for which the BH loops have been plotted in Fig. 3.

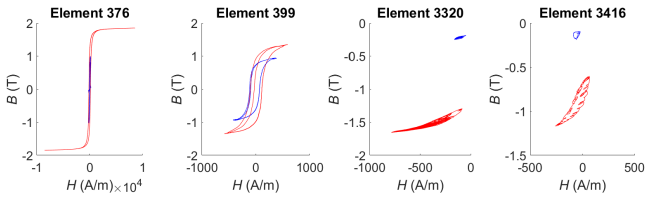

Fig. 3. The simulated BH behavior at two elements in the stator and two elements in the rotor as specified in Fig. 2. The blue curves are for the x-component and the red curves for the y-components of the flux density. The effect of the asynchronous field is seen as a double loop in some of the stator elements (399) and as biased hysteresis minor loops in some of the rotor elements.

TABLE I
PARAMETERS OF THE ANALYZED MACHINE

Parameter	SynRM
Power	4.8 kW
Voltage (main/additional)	190/40 V
Rated current (main/additional)	31/1 A
No-load current (main)	21.9 A
Connection (main/additional)	star/star
Frequency	50 Hz
Pole pairs (main/additional)	2/1
Stator outer diameter	235 mm
Stator inner diameter	145 mm
Number of slots	36
Airgap	1 mm

IV. Results and Discussion

The machine under investigation has been simulated with the above-mentioned methodology under voltage supply for both the main and the levitation windings. To operate the machine at no-load, the load angle is adjusted by fixing the rotor angle while computing with the SV model. The main winding voltage was fixed to 190 V and the additional winding voltage to 40 V. After fixing the no-load operation points from the SV model, the same operation points were used to simulate the motor with the hysteresis model. However, with the increasing additional winding current and

thus the levitation field, the saturation of the rotor changes slightly. The machine ideally operates at 40 V along the additional winding for full levitation, but to see the effect of the additional winding, the simulations have been carried out up to 250 V. The magnetic flux density for the machine at the no-load operation point under levitation is shown in Fig. 4. Here, the effect of the additional winding can be seen as a difference in the flux density distribution between the upper and lower parts of the machine. This difference is what creates the levitation force.

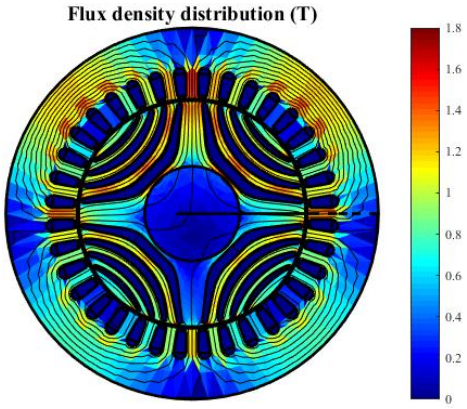

Fig. 4. The no-load flux density distribution in the cross section area of the machine. The difference between the upper and lower parts is what generates the levitation force due to the unbalanced magnetic pull.

The simulated magnetic behavior of the iron core under hysteresis and eddy current is analyzed at two elements in the stator core and two elements in the rotor core as shown in Fig. 3, where the blue curves are for the x-component and the red curves for the y-components of the flux density. Here, one can see that in the stator, the hysteresis loops are doubled as the flux density changes with the additional winding current, which is a two-pole winding, whereas the main winding is a four-pole winding. Furthermore, the effect of the main flux bias and the varying levitation flux are seen in the rotor core. Part of the losses related to the rotor hysteresis loops are the main cause of torque production due to the additional winding. The plots show the last 2 periods after reaching steady state.

The computed iron losses in the stator and rotor of the machine are shown in Fig. 5. In these cases, the additional winding is supplied from 0 V to 250 V, while the main winding is kept at 190 V and the losses are plotted against the additional winding current.

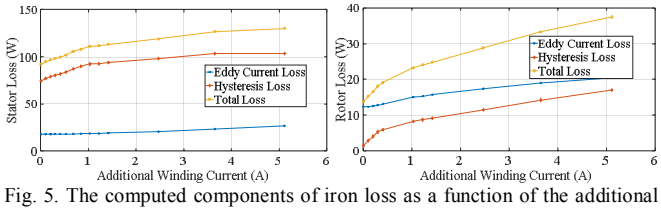

Fig. 5. The computed components of iron loss as a function of the additional winding current. Even at zero additional current, losses are seen in the rotor although the main flux is only synchronous. These losses are associated with the flux density harmonics coming from the slotting and flux barriers.

Fig. 5 shows that the additional winding has a significant impact on the losses of the machine in both rotor and stator. The losses in the rotor are different from zero even at zero additional current. However, these losses do not generate any positive torque, as they are associated with the flux density harmonics. The increase of the stator core losses is due to the harmonics (with respect to the main flux) induced by the additional winding. The increase of the rotor losses is due to both the fundamental harmonic of the levitation flux and its harmonics. When the additional winding is energized, an increase in the shaft power was observed in the computations with both SV and MDVH models. This is explained by the saturation of iron, which shifts the flux form the d-axis of the machine. This shift depends on the model used and thus makes the comparison between the two models challenging. A good way to compare the simulations is as follows. In the SV simulations, the iron losses are not accounted for and thus they show as extra shaft power, when it is computed from the torque and the speed. In the case of MDVH computations, the iron losses are accounted for in the power balance of the whole machine. The copper losses in both cases are accounted for, thanks to the field-circuit coupling. Thus to have a better appreciation of the hysteresis torque related shaft power, we needed to subtract the iron losses from the computed shaft power in the case of SV simulations and then compute the difference between this shaft power and the one computed with the MDVH model as:

$$P_{\text{diff}} = P_{\text{sh-MDVH}} - \left(P_{\text{sh-SV}} - P_{\text{Fe}}\right) \tag{1}$$

where P stands for power and the subscripts *sh* for shaft, *SV* for single-valued, FE for iron, and MDVH for magneto-dynamic vector hysteresis. SV and MDVH refer to the modelling methodology.

The computed results from (1) are shown in Fig. 6, together with the increase of iron losses in the rotor as a function of the additional winding current. This comparison is motivated by the analytical description of an induction machine, where the so-called airgap power P_{ag} is split into two parts according to the slip s of the machine. The first part $(1\text{-}s)P_{\text{ag}}$ is the mechanical power, whereas the second part sP_{ag} is the rotor loss. Since the slip associated with the levitation field in this case is 50%, this means that the airgap power is split into two equal parts, the mechanical power and the rotor losses. From Fig. 6, one can see that these powers have the same trend and they match each other very well at low values of the additional winding current. However, when the current is large, the difference between the two powers increase. This behavior is understandable as the analytical model is based solely on the fundamental component of the flux density in the airgap. Indeed, when the additional winding current is increasing, the fundamental component of the flux density associated with it increases too and produces positive torque. However, the higher harmonics also increase and produce positive or negative torque depending on their rank and direction of rotation with respect to the rotor. Thus, not all the rotor losses are associated with a positive torque.

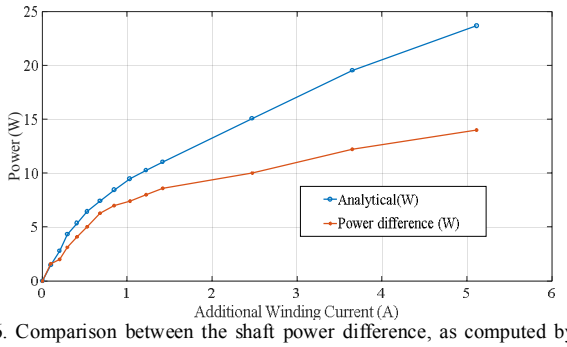

Fig. 6. Comparison between the shaft power difference, as computed by the MDCH and SV models according to equation (1) and the analytical equation from the equivalent circuit model of an induction machine. The trend is similar but the analytical equation overestimate the power as it is based on the fundamental harmonic only.

To confirm the above results, we made a simple experiment on the prototype shown in Fig. 7a. We present it here as a proof of concept rather than a validation. In the experiment, the main winding of the motor was connected to a sinusoidal power supply from the grid, and the amplitude of the voltage was increased slowly with an autotransformer. The rotor and the shaft were kept levitated by the active magnetic bearings, which reduces the friction loss in the system. The rotor started rotating at 28 V, with a terminal current of 5.4 A. The starting current was much higher and fluctuated heavily. The steady state measured speed was 744 rpm, which means that the SynRM was rotating as an asynchronous motor. To get an estimate of the torque in this experiment, we carried out a FE computation with the MDVH model with the same supply voltage and speed. The computed terminal current and torque were 5.27 A and 0.13 Nm. To obtain the same torque by energizing the additional winding instead of the main windings, approximately the same current would be needed as seen in the computations of Fig. 7b. These computations were carried out with a blocked rotor. Such a high current was not possible to implement on the prototype, as the risk of damage it is evident.

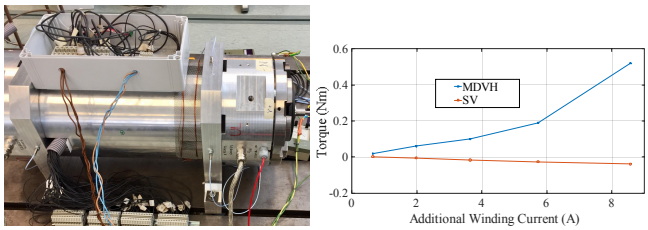

(a) (b)

Fig. 7. a) Measurement setup with the prototype motor. The large parts at the end of the prototype are active magnetic bearings. b) Computed torque vs additional winding current in blocked rotor condition with the main winding open. The MDVH model shows an increasing torque, whereas the SV model shows decreasing one.

V. Conclusion

Through well-designed computations with an advanced hysteresis and eddy current model, the paper showed that the asynchronous field in bearingless synchronous machines produces a positive torque that adds to the motoring one. Furthermore, it shows that this torque can be roughly approximated by the classical equivalent circuit model of an asynchronous machine, in which the airgap power is split into rotor losses and shaft power in the proportions *s* and 1-*s*, *s* being the slip of the rotor with respect to the levitation field. Such a result could have an impact on the control of the machine especially in case of sensorless control.

In the hysteresis model, the magnetic field associated with the excess losses was ignored. Such an approximation still need to be investigated in view of more accurate computations. Further, we carried out a simple test and presented it as a proof of concept. A thorough experimental validation of the presented results is still needed. These issues will be at the focus of future works.

Acknowledgment

P. Rasilo, F. Martin and V. Mukhrejee acknowledge the Academy of Finland for financial support. This work was supported in part by the Estonian Research Council under the Grant number PUT1260.

References

[1] https://search-ext.abb.com/library/Download.aspx?DocumentID=3AUA0000132610&LanguageCode=en&DocumentPartId=&Action=Launch

[2] M. Ferrari, N. Bianchi, A. Doria and E. Fornasiero, "Design of synchronous reluctance motor for hybrid electric vehicles," *IEEE Transactions on Industry Applications*, vol. 51, no. 4, pp. 3030-3040, July-Aug. 2015.

[3] M. Takemoto, K. Yoshida, N. Itasaka, Y. Tanaka, A. Chiba and T. Fukao, "Synchronous Reluctance Type Bearingless Motors with Multi-flux Barriers," *2007 Power Conversion Conference - Nagoya*, Nagoya, 2007, pp. 1559-1564.

[4] T. Reichert, T. Nussbaumer and J. W. Kolar, "Bearingless 300 W PMSM for bioreactor mixing," *IEEE Transactions on Industrial Electronics*, vol. 59, no. 3, pp. 1376-1388, March 2012.

[5] W. Amrhein, S. Silber and K. Nenninger, "Levitation forces in bearingless permanent magnet motors," *IEEE Transaction on Magnetics*, vol. 35, no. 5, pp. 4052-4054, September 1999.

[6] Masahide Ooshima and Chiharu Takeuchi, "Magnetic Suspension Performance of a Bearingless Brushless DC Motor for Small Liquid Pumps," *IEEE Transactions on Industry Applications*, vol. 47, no. 1, pp. 72-78, March 2011.

[7] A. Belahcen, V. Mukherjee, M. F. Far, P. Rasilo and M. Hinkkanen, "Coupled field and space-vector equations of bearingless synchronous reluctance machine," *XXII International Conference on Electrical Machines (ICEM)*, Lausanne, 2016, pp. 2581-2587.

[8] P. I. Koltermann, J. P. A. Bastos, N. Sadowski, N. J. Batistela, A. Kost, L. Janicke and K. Miethner, "Nonlinear magnetic field model by FEM taking into account hysteresis characteristics with M-B variables," *IEEE Transaction on Magnetics*, vol. 38, no. 2, pp. 897-900, March 2002.

[9] L. Zhu and C. S. Koh, "A Novel Vector Hysteresis Model Using Anisotropic Vector Play Model Taking Into Account Rotating Magnetic Fields," *IEEE Transactions on Magnetics*, vol. 53, no. 6, pp. 1-4, June 2017.

[10] E. Dlala, A. Belahcen, K. A. Fonteyn and M. Belkasim, "Improving loss properties of the Mayergoyz vector hysteresis model," *IEEE Transactions on Magnetics*, vol. 46, no. 3, pp. 918-924, March 2010.

[11] S. E. Zirka, Y. I. Moroz, R. G. Harrison and N. Chiesa, "Inverse Hysteresis Models for Transient Simulation," *IEEE Transactions on Power Delivery*, vol. 29, no. 2, pp. 552-559, April 2014.

[12] S. E. Zirka, Y. I. Moroz, N. Chiesa, R. G. Harrison and H. K. Høidalen, "Implementation of Inverse Hysteresis Model Into EMTP—Part II: Dynamic Model," *IEEE Transactions on Power Delivery*, vol. 30, no. 5, pp. 2233-2241, Oct. 2015.

[13] I. D. Mayergoyz, *Mathematical Models of Hysteresis and Their Applications*. New York: Aca. Pre. Ser. Elect., 2003.

[14] D. Singh, F. Martin, P. Rasilo and A. Belahcen, "Magnetomechanical Model for Hysteresis in Electrical Steel Sheet," *IEEE Transactions on Magnetics*, vol. 52, no. 11, pp. 1-9, Nov. 2016.